7

Silicon Nanocrystals

Hong Yu, Jie-qiong Zeng and Zheng-rong Qiu
Southeast University
China

1. Introduction

Silicon has many advantages over other semiconductor materials: low cost, nontoxicity, practically unlimited availability, and decades of experience in purification, growth and device fabrication. It is used for almost all modern electronic devices. However, the indirect energy gap in bulk crystalline Si makes it unable to emit light efficiently and thus unsuitable for optoelectronic applications. For example, lasers, photodetectors are not constructed from silicon. On the other hand, although silicon is widely used for solar cell fabrication, the efficiency can not exceed the Schockley and Queisser limit in single band gap device, because of its inability to absorb photons with energy less than the band gap and thermalisation of photon energy exceeding the band gap. One approach for tackling this disadvantage is to use tandem cells, which can implement the increasing of the number of band gaps (Conibeer et al., 2006; Cho et al., 2008). Moreover, the band gap in silicon is too small to interact effectively with the visible spectrum. If the gap could be adjusted, silicon would be used for either electronic or optical application. In 1990, it was firstly observed experimentally by Canham (Canham, 1990), that photoluminescence (PL) occurs in the visible range at room temperature in porous silicon (PS). Since then the silicon clusters or silicon quantum dots (Si-QDs) or silicon nanocrystals (Si-NCs) have attracted much of research interest, and many of theoretical models, computations, and experimental results on band structures, PL and other electronic properties have been reported during the last decades (Öğüt et al., 1997; Fang & Ruden, 1997; Wolkin et al., 1999; Wilcoxon et al., 1999; Soni et al., 1999; Vasiliev et al., 2001; Garoufalis & Zdetsis, 2001; Carrier et al., 2002; Nishida, 2004; Biteen et al., 2004; Tanner et al., 2006). The results from these reports show that in low-dimension silicon structures, such as silicon nanocrystals or silicon quantum dots, electronic and optical properties can be quite different from those of silicon bulk counterpart, for instance, free-standing Si-NCs show strong luminescence, the color of which depends on the size of the Si-NCs, and the gap and energy increase when their size is reduced. Therefore, the energy gap can be tuned as a function of the size of quantum dots.

We are especially interested in the theoretical study on the band gap and the optical spectrum with respect to the size of the Si-NCs or Si-QDs and surface terminations and reconstructions.

The effective mass approximation (EMA) is used by Chu-Wei Jiang and M. Green to calculate the conduction band structure of a three-dimensional silicon quantum dot superlattice with the dots embedded in a matrix of silicon dioxide, silicon nitride, or silicon carbide(Jiang & Green, 2006), and later the EMA is only of partial use in determining the absolute confined energy levels for small Si-NCs, because it has been found a decreasingly

accurate prediction of the confined energy level by the EMA as the Si-QDs size decreases(Conibeer et al., 2008).

Time dependent density functional theory (TDDFT) has been performed by Aristides D. Zdetsis and C. S. Garoufalis over the last ten years (Garoufalis & Zdetsis, 2001; Zdetsis & Garoufalis, 2005). In their calculations the Si dangling bonds on the surface of the Si-NCs are passivated by hydrogen and oxygen. In the DFT method, they have used the hybrid nonlocal exchange correlation functional of Becke and Lee, Yang and Parr, which includes partially exact Hartree–Fock exchange (B3LYP). Their results are in excellent agreement with accurate recent and earlier experimental data. It is found that the diameter of the smallest oxygen-free nanocrystal that could emit PL in the visible region of the spectrum is around 22 Å, whereas the largest diameter falls in the range of 84– 85 Å. The high level and the resulting high accuracy of their calculations have led to the resolution of existing experimental and theoretical discrepancies. Their results also clarify unambiguously and confirm earlier predictions about the role of oxygen on the gap size. More recently, they report accurate high level calculations of the optical gap and absorption spectrum of ultra small Si-NCs of 1nm, with hydrogen and oxygen passivation (with and without surface reconstruction) (Garoufalis & Zdetsis, 2009). They show that some of the details of the absorption and emission properties of the 1 nm Si nanoparticles can be efficiently described in the framework of TDDFT/B3LYP, by considering the effect of surface reconstruction and the geometry relaxation of the excited state. Additionally, they have examined the effect of oxygen contamination on the optical properties of 1nm nanoparticles and its possible contribution to their experimentally observed absorption and emission properties.

By performing the same method, TDDFT, the optical absorption of small Si-NCs embedded in silicon dioxide is studied systematically by Koponen (Koponen et al., 2009). They have found that the oxide-embedded Si-NCs exhibit absorption spectra that differ significantly from the spectra of the hydrogen-passivated Si-NCs. In particular, the minimum absorption energy is found to decrease when the Si-NCs are exposed to dioxide coating. The absorption energy of the oxide-embedded Si-NCs remains approximately constant for core sizes down to 17 atoms, whereas the absorption energy of the hydrogen-passivated Si-NCs increases with decreasing crystal size. They suggest a different mechanism for producing the lowest-energy excitations in these two cases.

Wang, et al, generate and optimize geometries and electronic structures of hydrogenated silicon nanoclusters, which include the T_d and I_h symmetries by using the semi-empirical AM1 and PM3 methods, the density functional theory DFT/ B3LYP method with the 6-31G(d) and LANL2DZ basis sets from the Gaussian 03 package, and the local density functional approximation (LDA), which is implemented in the SIESTA package(Wang et al., 2008). The calculated energy gap is found to be decreasing while the diameter of silicon nanocluster increases. By comparing different calculated results, they conclude that the calculated energy gap by B3LYP/6-31G(d)//LDA/SIESTA is close to that from experiment. For investigation of the optical properties of Si-NCs as a function of surface passivation, they carry out a B3LYP/6-31G(d)//LDA/SIESTA calculation of the Si_{35} and Si_{47} core clusters with full alkyl-, OH-, NH_2-, CH_2NH_2-, OCH_3-, SH-, C_3H_6SH-, and CN- passivations. In conclusion, the alkyl passivant affects the calculated optical gaps weakly, and the electron-withdrawing passivants generate a red-shift in the energy gap of silicon nanoclusters. A size-dependent effect is also observed for these passivated Si nanoclusters.

The optical absorption spectra of Si_nH_m nanoclusters up to 250 atoms are computed using a linear response theory within the time-dependent local density approximation (TDLDA)

(Vasiliev et al., 2001). The TDLDA formalism allows the electronic screening and correlation effects, which determine exciton binding energies, to be naturally incorporated within an ab initio framework. They find the calculated excitation energies and optical absorption gaps to be in good agreement with experiment in the limit of both small and large clusters. The TDLDA absorption spectra exhibit substantial blueshifts with respect to the spectra obtained within the time-independent local density approximation.

2. Structure of silicon quantum dots

Typically, the size of Si-QDs is less than ten nanometers which is close to the exciton Bohr radius of bulk silicon. Owing to the extreme small dimensions, silicon quantum dots exhibit strong quantum confinement which causes the band gaps to widen, the electronic states to become discrete, and the oscillator strength of the smallest electronic transitions to increase. Generally, at ideal conditions, we consider that the interior of the dot has the structure of crystalline silicon while the surface of the dot is passivated with specific atoms depending on the surrounding environment of the dot, such as hydrogen, oxygen and so on.

2.1 Physical characterization

Direct physical evidence of the crystallinity of Si-QDs has been obtained from high resolution TEM, see Fig. 1a and b (Conibeer et al., 2006). Crystal planes are apparent in many of the darker areas in these HRTEM images. The darker areas are denser material in a less dense matrix, which are attributed to Si-NCs in a SiO_2 matrix.

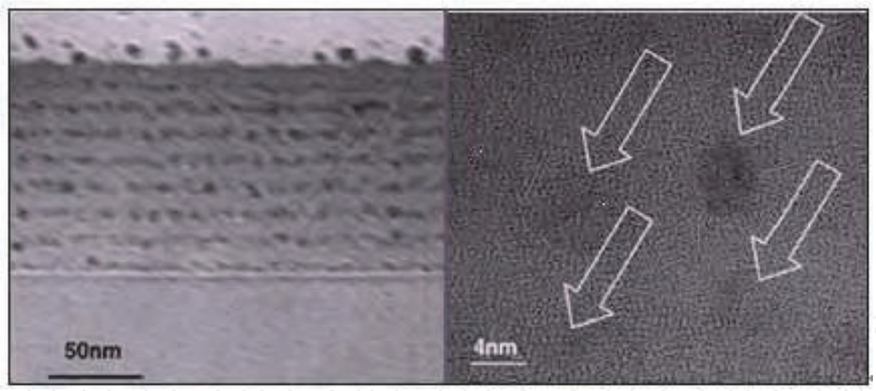

(a) (b)

Fig. 1. Cross-sectional TEM (a) HRTEM (b) images of Si QDs in oxide. (a) Shows the layered structure and (b) shows individual nanocrystals in which crystal planes can be seen

Scientists also have studied about the nanostructures of Si QDs in other dielectrics such as silicon nitride and silicon carbide, see Fig. 2a and b (Conibeer et al., 2006, 2008). Results from HRTEM images are very promising, showing crystalline nanocrystals in the nitride matrix and carbide matrix.

From the introduction stated above, we can see that it is reasonable to suppose that the interior of the dot has the structure of crystalline silicon while the surface of the dot is passivated with specific atoms at ideal conditions.

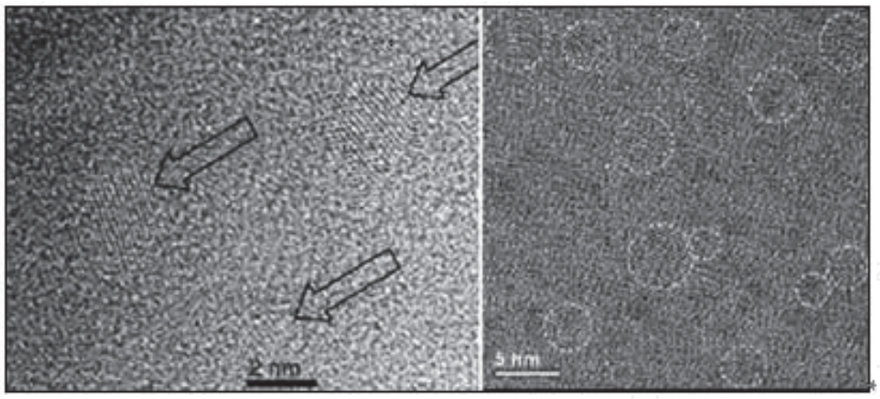

(a) (b)

Fig. 2. HRTEM images of Si-QDs in (a) silicon nitride and (b) silicon carbide

2.2 Ideal structure

Lots of experimental researches have been made on the electronic and optical properties of Si-QDs. However, several factors contribute to making the interpretation of measurements a difficult task. For instance, samples show a strong dispersion in the QD size that is difficult to be determined. In addition, Si-NCs synthesized by different techniques often show different properties in size, shape and the interface structure (Guerra et al., 2009). For the reasons stated above, the majority of experimental work give diverse results. Therefore, theoretical model calculations for some ideal structures have been considered very necessary to investigate the properties of Si-QDs. Generally, passivated-surface silicon nanoclusters are the ideal theoretical structure for us to study Si-QDs. In this section, we will introduce several ideal structures of Si-QDs in theoretical simulation.

2.2.1 Hydrogen-passivated silicon quantum dots

Hydrogen is often used as the passivating agent for the silicon nanocluster surface in most of the theoretical calculations and computations. It is generally accepted that hydrogen-passivated silicon nanocluster (Si_nH_m cluster) is the simplest structure to represent Si-QDs in a vacuum environment and can reproduce most of the experimental results in despite of neglecting some interface effects.

In Fig. 3, some idealized hydrogen-passivated quantum dots of silicon are illustrated. The interior of the dot consists of silicon atoms in the diamond structure; the surface of the dot is hydrogen-passivated. We can see that hydrogen atoms remove all dangling bonds on the surface.

2.2.2 Oxidized silicon quantum dots

Si-QDs are believed to be the luminescence centres in PS. Experimental measurements on PS samples have indicated that a large PL redshift is observed as soon as the freshly etched samples (oxygen-free PS) are transferred from Ar to a pure oxygen atmosphere or to air; however, no redshift at all is detected when the samples are kept in pure hydrogen atmosphere or in vacuum (Wolkin et al., 1999). Therefore, it is obviously that the chemistry of oxygen at the surface has played an important role when PS is exposed to air and has to be considered in theoretical models for this problem.

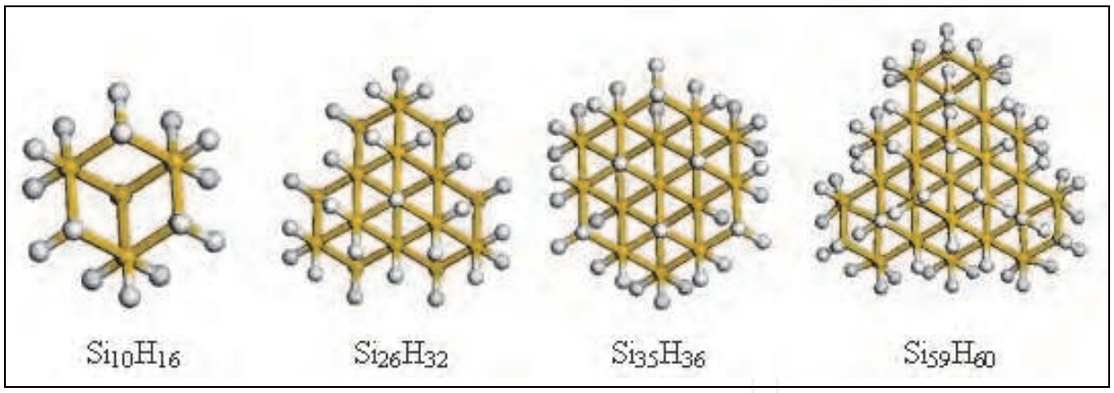

Fig. 3. Structures of Si_nH_m clusters represented in terms of ball-and-stick models. Yellow balls denote Si atoms and the white balls denote surface H atoms

There are totally four possible oxygen passivations on the surface of Si-QDs: (i) double-bonded, (ii) backbonded, (iii) bridge-bonded and (iiii) inserted oxygen configurations. The ball and stick representations of these oxygen passivation configurations are illustrated in Fig. 4. Compared with corresponding hydrogen-passivated silicon clusters, oxidized clusters are built up by substituting H or Si atoms on the surface with oxygen. From (b) to (e), they are double-bonded, backbonded, bridge-bonded and inserted oxygen configurations, respectively. It should be noted that the backbonded oxygen configuration is different in geometry from the bridge-bonded oxygen configuration, in that the former can preserve hydrogen coverage on a Si nanocrystal and retain the number of Si atoms when it is oxidized, while in the latter, one oxygen atom replaces a surface SiH_2 dihydride on the initial dot causing a decrease of the number of H and Si atoms. In another word, for the backbonded oxygen configuration, the oxygen atom is situated between the nearest-neighbor Si atoms while in the bridge-bonded oxygen configuration it is situated between the second nearest-neighbor Si atoms, referring Fig. 4(c) and (d).

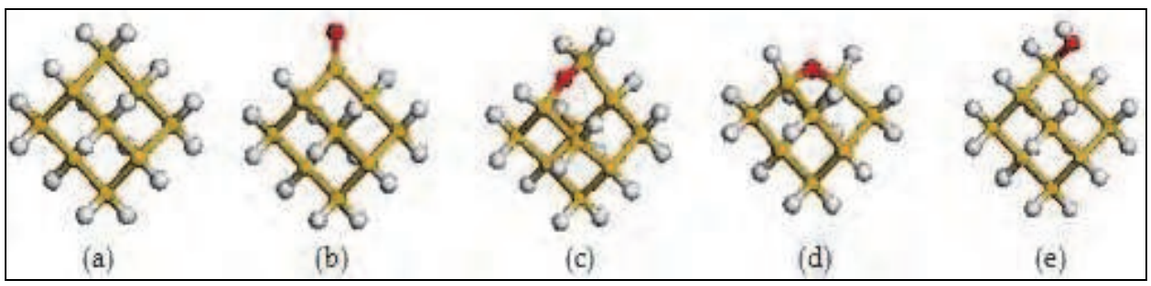

Fig. 4. Ball and stick representations of four possible oxygen passivation configurations, the yellow balls represent Si atoms, red balls represent O atoms, and the white balls, H atoms: (a) initial hydrogen-passivated silicon cluster, (b) double-bonded oxygen passivation configuration (c) backbonded (d) bridge-bonded (e) inserted oxygen configuration

Actually there may exist other oxygen-contamination on the surface of Si-QDs when oxidized. Zdetsis and Garoufalis (Zdetsis & Garoufalis, 2005) proposed a structure that can maintain the Td symmetry of the nanocrystals, considering only double-bonded oxygen configuration, see Fig. 5.

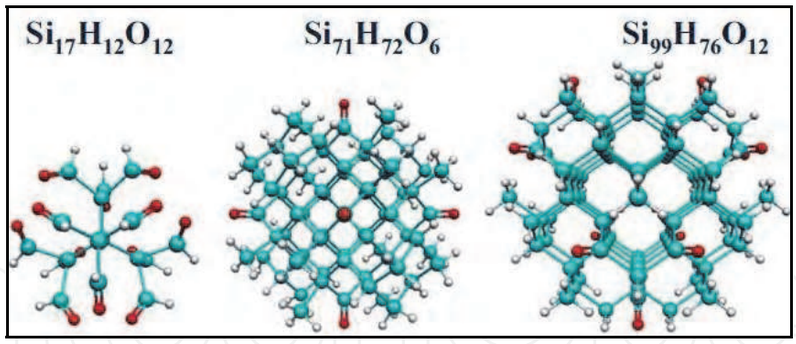

Fig. 5. Structure of oxidized nanocrystals with Td symmetry: The blue spheres are Si atoms, the red spheres are O atoms, and the white spheres are H atoms

2.2.3 Silicon quantum dots embedded in different matrixes

Si-QDs are often embedded in a dielectric matrix based on the fabrication of Si-QDs. Therefore, it is necessary to build an appropriate structure to simulate Si-QDs in such kind of environment.

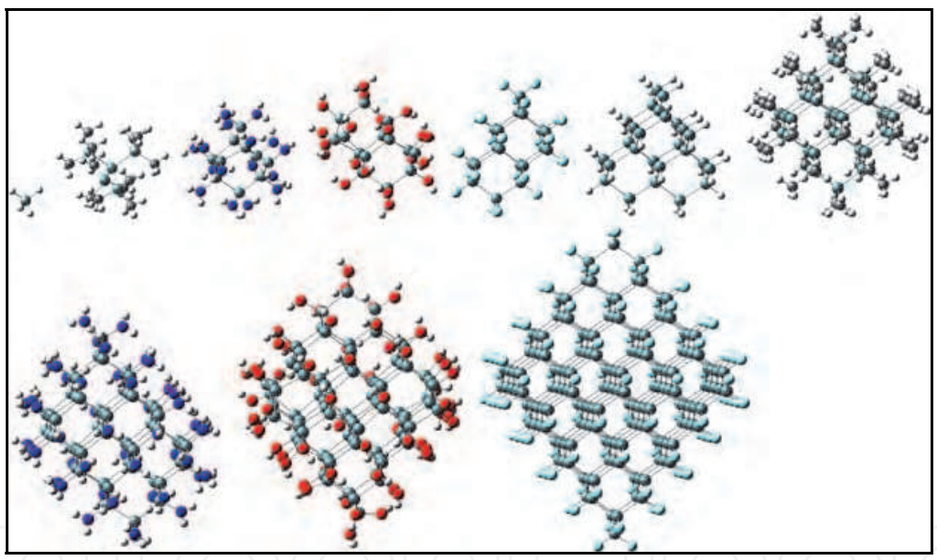

Fig. 6. Structures of Si-QDs embedded in an ionic environment, SiO_2, Si_3N_4, SiC matrix and a co-valent environment (left to right; top to bottom): SiH_4, $Si_5(CH_3)_{12}$, $Si_{10}(NH_2)_{16}$, $Si_{14}(OH)_{20}$, $Si_{18}F_{24}$, $Si_{26}H_{32}$, $Si_{35}(CH_3)_{36}$; $Si_{53}(NH_2)_{48}$, $Si_{84}(OH)_{64}$, $Si_{165}F_{100}$

König et al (König et al., 2009) have used F, OH, NH_2, CH_3 and H groups as the passivating agent for the Si clusters surface to simulate Si-QDs embedded in an ionic environment, SiO_2, Si_3N_4, SiC matrix and a co-valent environment, respectively, see Fig. 6. Apparently, these structures are simply built by replacing all the hydrogen atoms on the surface of hydrogen-passivated Si clusters with F, OH, NH_2 and CH_3 groups, respectively.

However, there are many more complex structures when Si-QDs embedded in a SiO_2 matrix. For instance, Koponen et al (Koponen et al., 2009) put forward some structures in which Si clusters are embedded in one or two neutral SiO_2 shells and the outermost layer of the cluster is hydrogen passivated in order to get rid of dangling bonds and to better mimic

the effect of bulk silicon oxide. One of these structures is presented in Fig. 7(a). In addition, Guerra et al (Guerra et al., 2009) obtained a crystalline embedded structure from a β-cristobalite (BC) matrix by removing all the oxygen atoms included in a cut-off sphere, whose radius determines the size of the Si-QDs. The final optimized structure of the Si_{32} in β-cristobalite matrix is illustrated in Fig. 7(b).

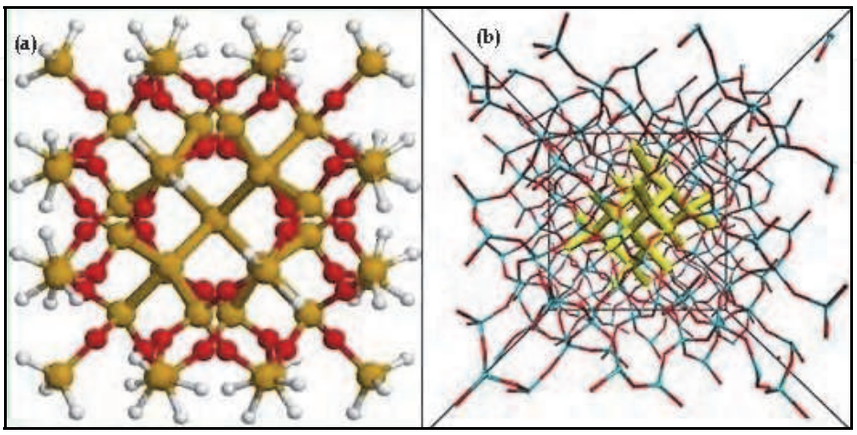

Fig. 7. (a) A stick and ball representation of $Si_{17}@Si_{24}O_{36}H_{60}$ (Si clusters embedded in one neutral SiO_2 shell), (b) The final optimized structure of the Si_{32} in β-cristobalite matrix

From the introduction stated above, we can clearly see that different structures should be used for simulating Si-QDs in different environment. Besides the structures presented above, there are many other structures used to simulate Si-QDs, we'll not elaborate here. It is crucial to choose an appropriate structure for a certain problem, otherwise the results may be inaccuracy and make no sense.

3. Method of calculation

Local-density approximations (LDA) are a class of approximations to the exchange correlation energy functional in DFT that depends solely upon the value of the electronic density at each point in space (and not, for example, derivatives of the density or the Kohn-Sham orbits). It was used to study on the band gap and PL of Si-QDs in early researches because of its simplicity and low computation cost. However, it is well known that time-independent LDA calculations typically underestimate the experimental photo-absorption gaps of Si-QDs (Vasiliev et al., 2001). TDLDA is then developed by Vasiliev as a natural extension of the ground state density-functional formalism and LDA, designed to include the proper representation of excited states.

The computation software we used is CASTEP module of Material Studio. CASTEP is an ab initio quantum mechanical program employing DFT to simulate the properties of solids, interfaces, and surfaces for a wide range of materials classes such as ceramics, semiconductors, and metals. First principle calculations allow researchers to investigate the nature and origin of the electronic, optical, and structural properties of a system without the need for any experimental input. It allows to choosing local, gradient-corrected, and non-local functionals for approximating exchange and correlation effect, and non-local functional include screened exchange, HF, B3LYP and PBE0. The screened exchange LDA (sX-LDA) is used to calculate the band structures of silicon quantum dots by considering the

computational cost and accuracy. The structures with hydrogen and oxygen passivations are partially shown in Fig. 3 and Fig.4, respectively.

4. Energy gaps of silicon quantum dots

Researches of Si-QDs can be divided into two groups: experimental measurements and theoretical simulations. The results of experiments are coincide with that of simulations to some extent, in spite of some discrepancies attributing to the measurement errors in experiments and the idealized structures in simulations. In this section, some results from other researchers are introduced first. Our computational results are then illustrated in the figures.

4.1 Experimental results

Very Large amounts of works have been done on light emission from Si-QDs because they are believed to be the luminescence centres in PS which had been observed having visible PL and electroluminescence at room temperature. Generally, the properties of Si-QDs are studied by measuring their PL in experiments. As we mentioned above, it is so hard to precisely control the purity and size of the sample that the results of different experiments may be differ from each other to some extent.

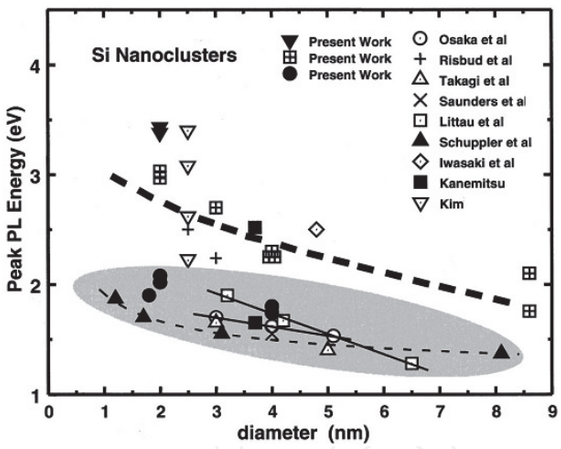

Fig. 8. Summary of experimental data on peak PL energy versus Si- QD size

Wilcoxon et al (Wilcoxon et al., 1999) had summarized most of the existing experimental results for PL peak energies as a function of the diameter of the Si-QDs, see Fig. 8. We note that there are differences in the dependence on size reported by different authors. As explained by Wilcoxon et al, all PL peaks of SiO_2 capped Si-QDs or Si-QDs embedded in glass matrices fall into the shaded region of the diagram while the experimental data for the oxygen-free samples (for the same value of the diameter) fall above this shaded region. So we can clearly see that the interface situation plays a significant role in the luminescence from Si-QDs.

In addition, Wolkin et al (Wolkin et al., 1999) obtained a similar conclusion by comparing the PL of PS samples in different atmosphere, see Fig. 9. They first examined the freshly etched samples (oxygen-free PS) with different porosities (equal to different sizes of Si-QDs) and emitting throughout the visible spectrum. Then the oxygen-free PS samples were

exposed to air and their PL energies were measured again. We can clearly see from Fig. 9 that after exposure to air, a redshift of the PL is observed, which can be as large as 1 eV for blue luminescent samples that contain QDs smaller than 2 nm. Besides, authors pointed out that a PL redshift was also observed as soon as the oxygen-free PS samples were transferred from Ar to a pure oxygen atmosphere while no redshift at all was detected when the samples were kept in pure hydrogen atmosphere or in vacuum. Moreover, they found that there is an upper limit of the emission energy (2.1 eV) which is independent of size. So the conclusion is that the surface passivation plays an important role, especially the chemistry of oxygen at the surface can cause an evident change on the PL of Si-QDs and an upper limit of energy gap.

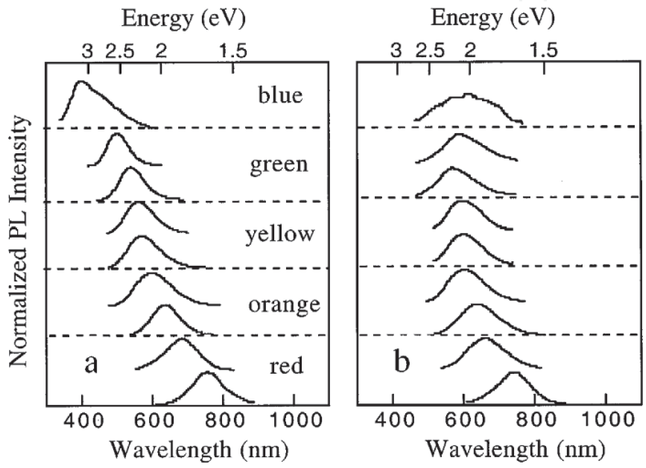

Fig. 9. Room temperature PL spectra from PS samples with different porosities kept under Ar atmosphere (a) and after exposure to air (b)

On the whole, despite some inevitable differences, the experimental results show that for ultra pure Si-QDs as their sizes decrease, there is a considerable blue-shift in the peak PL energy which is due to the increase of band gap. However, if the Si-QD is not pure enough, much more complex results will be obtained due to the influence of impurity contamination and complicate interface situation.

4.2 Theoretical calculation results

As we have mentioned above, a number of computations based on TDDFT, TDLDA, and other methods have been performed to simulate the properties of Si-QDs with different structures and passivations. In this section, we are going to introduce our calculation results and some theoretical results from other reports.

4.2.1 Hydrogen-passivated silicon quantum dots

Zdetsis and Garoufalis calculated the band gaps of hydrogen-passivated Si-QDs using TDDFT, the results are shown in Table 1 (Zdetsis & Garoufalis, 2005). As it can be easily seen in Table 1, with the size of Si-QDs decreases, the band gaps increases.

We have calculated the energy gaps of silicon QDs of different sizes from 0.6nm to 2nm in diameter by using the CASTEP computation program, which employ the plane-wave peseudopotentials method based on DFT. Some of the structures of Si-QDs we used are

shown in Fig. 3. In the computations, screening exchange LDA (sX-LDA)/CA-PZ is used as the type of exchange-correlation potential. As comparison, LDA/CA-PZ is selected as the type of DFT exchange-correlation potential and calculations are performed again. The results are shown in Fig. 10. It can be seen that LDA/CA-PZ suffer from the well-known underestimation of the energy gap while sX-LDA/CA-PZ can obtain a more accurate result which is well consistent with the results from other literatures (Vasiliev et al., 2001; Conibeer et al., 2006).

No. of Si atoms	Total No. of atoms	TDDFT[b] (eV)
5	17	6.66
17	353	5.03
29	65	4.53
35	71	4.42
47	107	4.04
71	155	3.64
99	199	3.39
147	247	3.19

Table 1. The band gaps for small Si nanoclusters

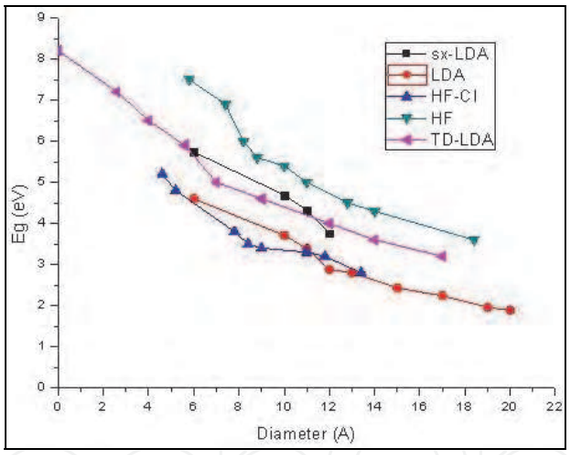

Fig. 10. Energy gaps of silicon QDs as a function of the QD diameter with H-termination from our work (■) & (●), and from the literatures [(▲) & (◀) from Vasiliev et al; (▼) from Conibeer et al]

4.2.2 Oxidized silicon quantum dots

Luppi and Ossicini (Luppi & Ossicini, 2005) carried out density-functional theory calculations on oxidized Si-QDs using local density approximation, considering three kinds of oxygen configurations: double-bonded, backbonded and bridge-bonded. The structures' schematic diagram has been shown in Fig. 4. They pointed out that the multiple presence of silanonelike Si=O bonds can be a reliable model for explaining the PL redshift observed in oxidized PS samples. The same conclusion has been reached by Zdetsis and Garoufalis (Zdetsis & Garoufalis, 2005) using TDDFT. Some of their calculated structures have been shown in Fig. 5.

However, a model based on a backbonded oxygen configuration has been proposed by Nishida to explain the observed PL redshift (Nishida, 2006). Nishida carried out self-consistent calculations using the extended Hückel-type non-orthogonal tight-binding method (EHNTB) for three different oxygen configurations (double-bonded, backbonded and inserted). The results are illustrated in Fig. 11. The author pointed out that the energy gaps calculated for Si dots double-bonded to oxygen are gradually decrease from 2.2 eV to about 1.7 eV with increasing dot size and the inserted oxygen configuration does not cause a significant energy-gap redshift even in the smallest Si-QD. At last he found out that the energy gaps calculated for the Si-QDs backbonded to oxygen coincide well with luminescence redshifts observed in PS.

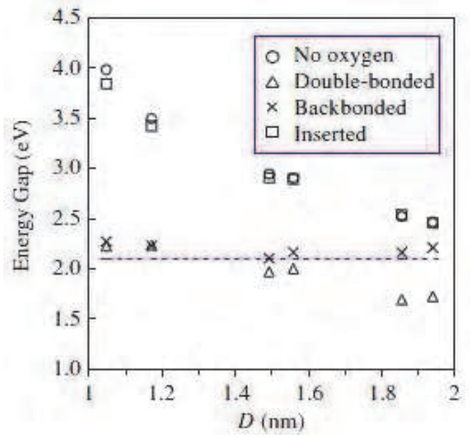

Fig. 11. Calculated energy gaps as a function of the diameter (D) of the Si -QDs studied. The dashed line shows the oxidation-induced peak energy (at ~2.1 eV) in PL spectra observed in PS

Obviously, the two conclusions stated above contradict each other. For this reason, we have performed calculations using the CASTEP computation program for all four kinds of oxygen configurations. The results we obtained based on LDA method are shown in Fig. 12, from which we can safely come to a conclusion that it is the formation of a Si=O double bond which is responsible for the PL redshifts in PS and other three types of oxygen configurations only cause a few decrease in energy gap.

The discrepancy between the above results may be due to the difference of the oxygen geometries, initial silicon clusters and the models based on different theories. So it is clear that different structures or models may obtain quite different results.

4.2.3 Silicon quantum dots embedded in different matrixes

König et al performed a systematic analysis of Si-QDs embedded in different environment by non-periodic spatial space density-functional–Hartree–Fock (DF–HF) computations of Si clusters comprising 1–165 Si atoms corresponding to a spherical QD diameter of d_{QD}=3.4–18.5Å (König et al., 2009). Some of the structures they used have been shown in Fig. 6 and their simulation results are illustrated in Fig. 13. Obviously, it shows that different interface termination causes different energy gaps. However, we can see that the entire trends of different interface terminations are the same. It is that the energy gap increase with the size decreasing.

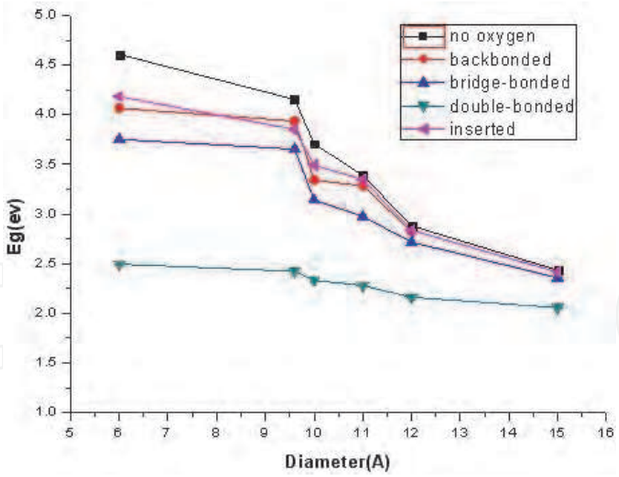

Fig. 12. Calculated energy gaps as a function of the diameter (D) of the Si-QDs

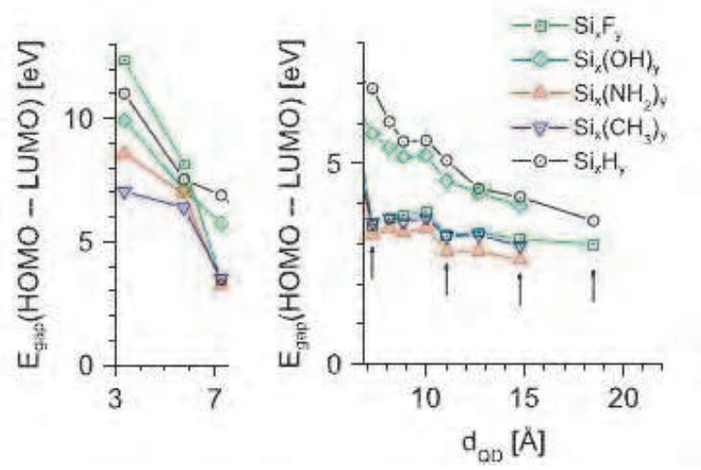

Fig. 13. Band gaps as a function of the diameter of Si-QDs with different interface terminations. For clarity, the graph is split into two sub-graphs with different energy scale. The points for the $Si_{10}X_{16}$ clusters (d_{QD} = 7.3 Å) are shown in both graphs

There are many more complicate calculations simulating Si-QDs in specific environments, we'll not list them one by one here. From the results above, we know that many factors will influence the properties of Si-QDs, other than the size, the interface termination also have a significant impact, so we should make an comprehensive considerations to study the properties of Si-QDs.

5. Conclusion

The band gap of Si-NCs or Si-QDs is size-dependent, and the energy of PL can be tuned from the near infrared to the ultraviolet by changing the size of nanocrystals. The surface passivation also plays an important role in determining the band gap. The third generation photovoltaic (PV) solar cell using tandem cells, which is based on Si quantum dots nanostructures, is proposed by Martin Green group (Conibeer et al., 2006, 2008). A number

of theoretical models, computations results on PL have been reported, and much of research effort on the properties of Si-QDs has been performing currently. Based on CASTEP quantum mechanical program with choice of sX-LDA/CA-PZ, the band gap of Si-QDs with H-passivation and O-passivation is calculated. The results show that band gap increases when the size of quantum dots decreases for both H-passivation and O-passivation structures. The computation method sX-LDA/CA-PZ is comparable with TDLDA in the computational accuracy. Further research on the band gap and PL of Si-QDs by choosing other non-local functional as the exchange correlation is in progress.

6. Acknowlegment

This work is partially supported by National High-Tech Research and Development Program of China under Grant No 2007AA04Z301.

7. Reference

Biteen, J. S.; Lewis, N. S., and et al. Size-dependen oxygen-related electronic states in silicon nanocrystals. *Applied Physics Letters*, Vol. 84 (2004), pp. 5389-5391

Canham, L. T.. Silicon quantum wire array fabrication by electrochemical and chemical dissolution of wafers. *Applied Physics Letters* , Vol.57 (1990), pp.1046-1048

Carrier, P. ; Lewis, L. J. and et al. Optical properties of structurally relaxed Si/SiO_2 superlattices : the role of bonding at interfaces. *Physical Review B*, Vol. 65, (2002), pp.165339-1—165339-11

Cho, E. C., Park, S. W., and et al. Silicon quantum dot/crystalline silicon solar cells. *Nanotechnology*, Vol.19, (2008), pp.1-5

Conibeer, G. ; Green, M. and et al. Silicon nanostructures for third generation photovoltaic solar cells. *Thin Solid Films,* Vol. 511-512 (2006), pp.654-662

Conibeer, G. ; Green, M. and et al. Silicon quantum dot nanostructures for tandem photovoltaic cells. *Thin Solid Films,* Vol. 516(2008), pp.6748-6756

Fang, T. N. & Ruden, P. P.. Electronic structure model for n- and p- type silicon quantum dots. Superlattices and Microstructures, Vol. 22 (1997), pp.590-596

Garoufalis, C. S. & Zdetsis, A. D.. High level Ab Initio calculations of the optical gap of small silicon quantum dots. *Physical Review Letters,* Vol. 87 (2001), pp.276402-1—276402-4

Garoufalis, C. S. & Zdetsis, A. D.. Optical properties of ultra small nanoparticals:potential role of surface reconstruction and oxygen contamination. *Journal of Math. Chem.*, Vol. 46 (2009), pp.952-961

Guerra, R.; Degoli, E. and et al. Size, oxidation, and strain in small Si/SiO2 nanocrystals. *Physical Review B,* Vol. 80 (2009), pp.155332-1—155332-5

Jiang, C. W. & Green, M. A.. Silicon quantum dot superlattices: modeling of energy bands, densities of states, and mobilities for silicon tandem solar cell applications. *Journal of Applied Physics*, Vol. 99(2006), pp.114902-1—114902-7

König, D.; Rudd, J. and et al. Impact of interface on the effective band gap of Si quantum dots. *Solar Energy Materials & Solar Cells*, Vol. 93 (2009), pp.753- 758

Koponen, L.; Tunturivuori, L. and et al. Effect of the surrounding oxide on the photoabsorption spectra of Si nanocrystals. *Physical Review B*, Vol. 79 (2009), pp.235332-1—235332-6

Luppi, M. & Ossicini, S.. Ab initio study on oxidized silicon clusters and silicon nanocrystals embedded in SiO2: Beyond the quantum confinement effect. *Physical Review B,* Vol. 71 (2005), pp.035340-1—035340-15

Nishida, M.. Electronic state calculations of Si quantum dots: Oxidation effects. *Physics Review B.*, Vol. 69 (2004), pp.165324-1—165324-5

Nishida, M.. Calculations of the electronic structure of silicon quantum dots: oxidation-induced redshifts in the energy gap. *Semicond. Sci. Technol.,* Vol. 21 (2006), pp.443–449

Öğüt, S. & Chelikowsky, J. R.. Quantum confinement and optical gaps in Si nanocrystals. *Physical Review Letters*, Vol. 79 (1997), pp.1770-1773

Soni, R. K.; Fonseca, L. F. and et al. Size-dependent optical properties of silicon nanocrystals. *Journal of Luminescence*, vol. 83-84 (1999), pp.187-191

Tanner, M. G.; Hasko, D. G. and et al. Investigation of silicon isolated double quantum-dot energy levels for quantum computation. Microelectronic Engineering, Vol. 83 (2006), pp.1818-1822

Vasiliev, I.; Chelikowsky, J. and et al. Ab initio absorption spectra and optical gaps in nanocrystalline silicon. *Physical Review Letters*, Vol. 86 (2001), pp.1813-1816

Wang, B. C.; Chou, Y. M. and et al. Structural and optical properties of passivated silicon nanoclusters with different shapes: a theoretical investigation. *Journal of Phys. Chem. A,* Vol. 112 (2008), pp.6351-6357

Wilcoxon, J.; Samara, G. and et al. Optical and electronic properties of Si nanoclusters synthesized in inverse micelles. *Physical Review B*, Vol. 60 (1999), pp.2704-2714

Wolkin, M.; Jorne, J. and et al. Electronic states and luminescence in porous silicon quantum dots: the role of oxygen. *Physical Review Letters*, Vol. 82 (1999), pp.197-200

Zdetsis, A. & Garoufalis, C.. Real space ab initio calculations of exitation energies in small silicon quantum dots, In : *Quantum Dots: Fundamentals, Applications, and Frontiers,* B. A. Joyce et al. (2005), pp.317–332

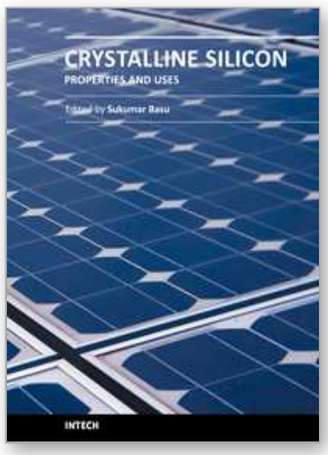

Crystalline Silicon - Properties and Uses

Edited by Prof. Sukumar Basu

ISBN 978-953-307-587-7
Hard cover, 344 pages
Publisher InTech
Published online 27, July, 2011
Published in print edition July, 2011

The exciting world of crystalline silicon is the source of the spectacular advancement of discrete electronic devices and solar cells. The exploitation of ever changing properties of crystalline silicon with dimensional transformation may indicate more innovative silicon based technologies in near future. For example, the discovery of nanocrystalline silicon has largely overcome the obstacles of using silicon as optoelectronic material. The further research and development is necessary to find out the treasures hidden within this material. The book presents different forms of silicon material, their preparation and properties. The modern techniques to study the surface and interface defect states, dislocations, and so on, in different crystalline forms have been highlighted in this book. This book presents basic and applied aspects of different crystalline forms of silicon in wide range of information from materials to devices.

How to reference

In order to correctly reference this scholarly work, feel free to copy and paste the following:

Hong Yu, Jie-Qiong Zeng and Zheng-Rong Qiu (2011). Silicon Nanocrystals, Crystalline Silicon - Properties and Uses, Prof. Sukumar Basu (Ed.), ISBN: 978-953-307-587-7, InTech, Available from: http://www.intechopen.com/books/crystalline-silicon-properties-and-uses/silicon-nanocrystals

INTECH
open science | open minds

InTech Europe
University Campus STeP Ri
Slavka Krautzeka 83/A
51000 Rijeka, Croatia
Phone: +385 (51) 770 447
Fax: +385 (51) 686 166
www.intechopen.com

InTech China
Unit 405, Office Block, Hotel Equatorial Shanghai
No.65, Yan An Road (West), Shanghai, 200040, China
中国上海市延安西路65号上海国际贵都大饭店办公楼405单元
Phone: +86-21-62489820
Fax: +86-21-62489821

IntechOpen